ACS APPLIED ENERGY MATERIALS

www.acsaem.org Article

Water-Assisted Increase of Ionic Conductivity of Lithium Poly(acrylic acid)-Based Aqueous Polymer Electrolyte

Jae Hyun Park,[▽] Sungyeb Jung,[▽] Yeon Hwa Song, Narayana R. Aluru, Taehoon Kim, Sang Bok Lee, U Hyeok Choi,* and Jaekwang Lee*

Cite This: *ACS Appl. Energy Mater.* 2020, 3, 10119−10130 Read Online

ACCESS | Metrics & More | Article Recommendations | Supporting Information

ABSTRACT: We propose a novel aqueous polymer electrolyte (APE) using a strongly hydrophilic poly(acrylic acid) (PAA) matrix containing mobile lithium counterions. The conductivity of this new PAA−Li^+−water electrolyte increases dramatically (to 10^{-2} S/cm at 298 K) with the addition of water. This value is almost 100 times higher than those of nonaqueous electrolytes and solid-state electrolytes. From the molecular dynamics simulations, we find that the increase of ion conductivity originates from the close interplay between ions, water, and the polymers in the molecule level. The structural features (i.e., ion/water distribution around the polymer) and transport properties (i.e., diffusion coefficient and ionic conductivity) are systematically investigated along with the quantifications of the microscopic properties such as the binding index of the ion, hydration numbers, and the equilibrium distance between the ion and PAA monomer at various water-content conditions. In particular, the change in the conductivity according to water content, ϕ_{Wt}, is divided into the diffusion-dominant regime at the low-water-content condition ($\phi_{Wt} < 0.7$) and the structure-dominant regime at the high-water-content condition ($\phi_{Wt} \geq 0.7$). In the diffusion-dominant regime, the conductivity increases by diffusion enhancement proportional to the water content, while in the structure-dominant regime, the conductivity varies little due to the considerable reduction of the number density of Li ions. Namely, there exists an optimal water content, above which the effects of additional water become negligible. We believe that our innovative findings would provide significant advances in developing APE-based high-power and long-life lithium-ion batteries. Also, the proposed nontoxic and flexible APE could offer a promising solution for the development of flexible and wearable aqueous rechargeable lithium-ion batteries.

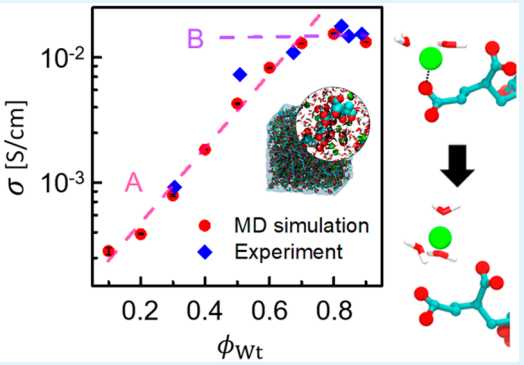

KEYWORDS: *aqueous polymer electrolyte, ionic conductivity, ionic diffusion, diffusion-dominant regime, structure-dominant regime, binding index, ion−water interaction, ion hydration structure*

1. INTRODUCTION

Since first commercialized by the Sony Corporation in 1991, the performance of lithium-ion batteries (LIBs) has been tremendously improved.[1−3] As a result, they are currently utilized as energy storage for diverse high-technology applications such as mobile phones, laptops, and electric vehicles.[4] However, there still exists an unresolved conflict with LIBs: a high-performance electrolyte versus safety. The organic-solvent-based liquid electrolytes used in conventional LIBs provide superior conductivity, one of the key factors for a high-performance battery, but this performance often comes with toxicity, volatilization, flammability, and explosions when such batteries are used under extreme conditions.[5] Those safety concerns could be avoided by replacing flammable liquid electrolytes in LIBs with solid-state electrolytes (SSEs). However, except several sulfide solid-state electrolytes, most SSEs have inherently lower ionic conductivity than liquid electrolytes do; therefore, current efforts are focused on improving their conductivity.[4] As one option to overcome these challenges, aqueous polymer electrolytes (APEs) have recently attracted considerable attention. This is due to their particular combination of advantages as an aqueous electrolyte (nonflammability, environmental friendliness, moisture insensitivity, and low cost)[6,7] and a polymer matrix (leakage-free feature, structural integrity, and flexible design possibility).[8] These characteristics make them ideal choices for use, even in wearable electronics.

In this study, we introduce a new single-ion Li^+-conducting APE and focus on the enhancement of the APE conductivity. The continuous addition of water to an APE that initially consists only of a polyanion matrix and lithium counter cations

Received: July 31, 2020
Accepted: September 16, 2020
Published: September 16, 2020

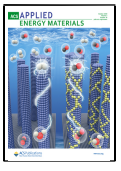

Scheme 1. Synthesis of (a) Vinyl Silica Nanoparticles (VSNs) and (b) Single-Li^+-Conducting Poly(acrylic acid)-Based APE Containing Silica Nanoparticles

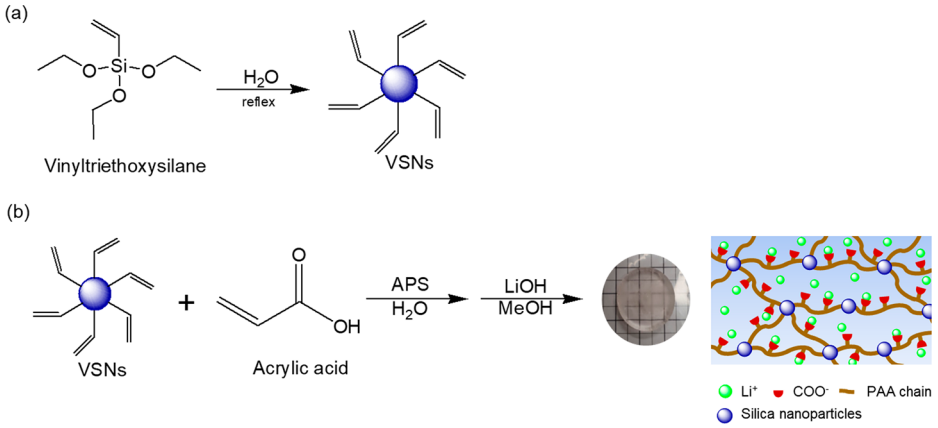

can cause a dramatic increase in ionic conductivity along with a state change from a rigid solid to a flexible gel. For the electrolyte with poly(ethylene oxide) (PEO) and either Li^+ or Na^+, as the medium is hydrated, its conductivity was reported to increase by as much as 1000 times that of a typical binary mixture of PEO and alkali metal salts (from 10^{-8} to 10^{-5} S/cm at room temperature).[9,10] However, even the improved conductivity is still 100 times lower than the minimum requirement for practical application. Considering that ion mobility is closely correlated with the surrounding water structure,[11,12] such a drastic change in the ionic conductivity through an aqueous polymeric matrix can be fully understood only by examining the microscopic interactions occurring within the polymer−water−ion system.[13,14]

The ion absorbing capability of a polymer, which is controlled by the polymer−ion interaction, is another key factor in determining the ionic conductivity of polymer-based electrolytes. To date, various polymer matrices, including PEO, poly(acrylonitrile) (PAN), poly(vinylidene fluoride) (PVDF), poly(methyl methacrylate) (PMMA), poly(vinyl alcohol) (PVA), and poly(vinyl chloride) (PVC), have been probed for the application to the polymeric electrolytes in LIBs.[15−18] The present study considers poly(acrylic acid) (PAA) as a host polymer. Compared to other polymer matrices, PAA is expected to solvate more Li ions, because it contains more oxygen atoms carrying negative charges in the monomer, and the structural complexity causing steric hindrance is relatively small.

Based on all the above, in this work, we present that the room temperature ionic conductivity of a PAA−Li^+−water electrolyte can be drastically enhanced (to the order of 10^{-2} S/cm) when an appropriate amount of water is added. This is confirmed in *in situ* experiments and supported by the results from a series of molecular dynamics (MD) simulations. The lithium single-ionic conductivities in this APE (>10^{-2} S/cm) are 10−100 times higher than the values of the nonaqueous electrolytes (NEs)[19] and NE-based SSEs,[20] and they are comparable to or higher than those of the aqueous electrolytes[7] and other APEs (9×10^{-3} S/cm).[21]

Although there have been previous works in which the influence of water dynamics and ion mobility in polymeric matrices has been investigated, most of the studies were conducted at a specific water content.[13,14,22,23] To our knowledge, a systematic study has not been performed on the conductivities at diverse water contents in the electrolyte. More specifically, little molecular understanding has been found out in the interplay between polymers, ions, and water that occurs as the amount of water varies. For example, what is the influence of the ion−water structure around polymers on the conductivity? How does the hydration number of ions vary with the addition of water?

2. EXPERIMENTAL SECTION

2.1. Experimental Procedure. For the experimental system, we prepared lithium single-ion-conducting PAA-based APEs containing silica nanoparticles, where PAA and silica nanoparticles act as the polymer matrix and chemical cross-linking points, respectively. Electrochemical impedance spectroscopy provided direct information about the ionic conductivity in the electrolytes with various water weight fractions ϕ_{Wt} = 0.3 to 0.9. Also, Figure S1 in the Supporting Information shows an example of the typical conductivity spectra, where the ionic conductivity value was obtained from the in-phase part of the conductivity.

2.2. Materials and Synthesis of APEs. Li^+ single-ion-conducting PAA-based APEs containing silica nanoparticles were synthesized via two-step processes (see Scheme 1), such as a sol−gel reaction and free radical polymerization. The sol−gel method was used to prepare vinyl silica nanoparticles (VSNs) acting as covalent cross-linking points (see Scheme 1(a)), thereby allowing for the creation of a solid-state network structure. Vinyltriethoxysilane (1.9 g, Tokyo Chemical Industry) was added into deionized water (15 mL). Then, the mixture was allowed to react overnight at room temperature, resulting in VSNs (whose average diameter is around 5 nm as shown in Figure S2 in the Supporting Information) dispersed in water. A solution of AA monomers (0.6 g, Sigma-Aldrich) in deionized water (1.4 mL) was added to the VSN dispersion solution (0.15 g). The mixture was stirred for 1 h, and then, ammonium persulfate (APS, 0.02 wt %, Alfa Aesar) as the initiator was added to the aqueous mixture. The temperature of the reaction mixture was maintained under 70 °C for 3 h to give a transparent solid-state VSN cross-linking PAA membrane (Scheme 1(b)). To neutralize the PAA membrane with Li^+, the product was soaked in a mixed solution of lithium hydroxide (LiOH, 1 g, Tokyo Chemical Industry) and methanol (MeOH, 100 mL, Duksan Reagents) for 5 days and then washed several times with MeOH and filtered to remove any unreacted LiOH. The Li^+-neutralized PAA membrane was dried at 40 °C for overnight to completely remove the solvent. The extent of neutralization (99% neutralized with Li^+) achieved from the ion exchange procedure was confirmed by elemental analysis from inductively coupled plasma mass spectrometry and pH value analysis (Figure S3). The various amounts of deionized water (31, 51, 67, 82, 85, and 89 wt %, listed in Table S1) were added to the sample to demonstrate the effect of water content on ionic conductivity. The additionally detailed experimental analyses of these materials were conducted using the

https://dx.doi.org/10.1021/acsaem.0c01765
ACS Appl. Energy Mater. 2020, 3, 10119−10130

rheological, thermal, and microstructural measurements. The Supporting Information contains the information on the PAA spacing between the silica nanoparticles ($M_x \approx 90\,100$ g/mol, Figure S4), glass transition temperature (T_g = 102 °C, Figure S5), silica nanoparticle distribution within the PAA matrix (Figure S6), and pH value (~6.36, Figure S7).

2.3. Ionic Conductivity Measurement. The ionic conductivity measurements of the APEs were performed by electrochemical impedance spectroscopy using a Bio-Logic VSP-300 multipotentiostat, with a 10 mV amplitude and 10^{-1}~10^{7} Hz frequency range. Samples were prepared by sandwiching them between two freshly polished brass top and bottom electrodes with 10 and 20 mm diameters, respectively. This created a parallel plate capacitor cell, and its precise thickness verification proceeded after the measurements were completed. Data were collected in isothermal frequency sweeps at room temperature. The complex dielectric $[\varepsilon^*(\omega) = \varepsilon'(\omega) - i\varepsilon''(\omega)]$ and conductivity $[\sigma^*(\omega) = \sigma'(\omega) + i\sigma''(\omega)]$ functions were obtained by measuring the complex impedance $[Z^*(\omega)]$ and given by

$$\varepsilon^*(\omega) = \frac{1}{C_0}\frac{1}{i\omega Z^*(\omega)} = \frac{L}{A\varepsilon_0}\frac{1}{i\omega Z^*(\omega)} \quad (1)$$

$$\sigma^*(\omega) = i\omega\varepsilon_0\varepsilon^*(\omega) \quad (2)$$

where C_0 is the vacuum capacitance, ω is the angular frequency, ε_0 is the vacuum permittivity, L is the distance between the electrodes, and A is the cross-sectional area of the top electrode. The ionic conductivity σ_{exp} is noted as the plateau region in the in-phase part of conductivity $\sigma'(\omega)$ as indicated by the dashed horizontal line in Figure S1.

3. MOLECULAR DYNAMICS SIMULATIONS

Along with the *in situ* experimental observation, the extensive MD simulations were performed to understand the mechanism of conductivity of the PAA−Li^+−water electrolyte. Figure 1 presents the molecular visualization of the PAA−Li^+−water electrolyte system used in this study at a representative water content of ϕ_{Wt} = 0.7. The water content, ϕ_{Wt}, is the mass fraction of water in the system, and it is expressed as

$$\phi_{Wt} = \frac{m_{Wt}}{m_{PAA} + m_{Wt} + m_{Li}} \quad (3)$$

where m_{PAA}, m_{Wt}, and m_{Li} are the mass of PAA, water, and the lithium ion, respectively. In all the MD simulations, the number of PAA molecules and Li ions (Li^+) are kept constant as 27 and 2484, respectively. Each PAA molecule has 92 periodic monomers. The number of Li^+ was determined for the system to be fully neutralized with the assumption that all acid groups are ionized and neutralized 100% with lithium. It is based on the observation that the extent of neutralization with lithium cations in the present electrolyte appeared as 99% (see Section 2.2). PAA was modeled with a united atom model, and the atomic charges and Lennard−Jones (LJ) parameters were taken from the values in GROMOS force field.[24] The waters were modeled with the SPC/E model.[25] The LJ parameters for Li^+ were taken from the Dang parameter.[11,12,26] All the MD simulations were performed with GROMACS 4.6.7.[27] For the MD simulations, initially PAA molecules, Li^+, and water molecules were put together in a sufficiently large simulation box according to the given water content at high temperature of T = 1000 K. Then, an annealing process was applied to obtain an equilibrium system at pressure of p = 1.0 atm and T = 300 K. At the end of the process, the system was equilibrated with an NPT ensemble for 5.0 ns. The system temperature and pressure were regulated with a Nosé−Hoover thermostat[28,29] and Parrinello−Rahman barostat,[30,31] respectively. Finally, the simulation was proceeded for 40 to 90 ns more to produce the data. The time step for the simulations was 1.0 fs.

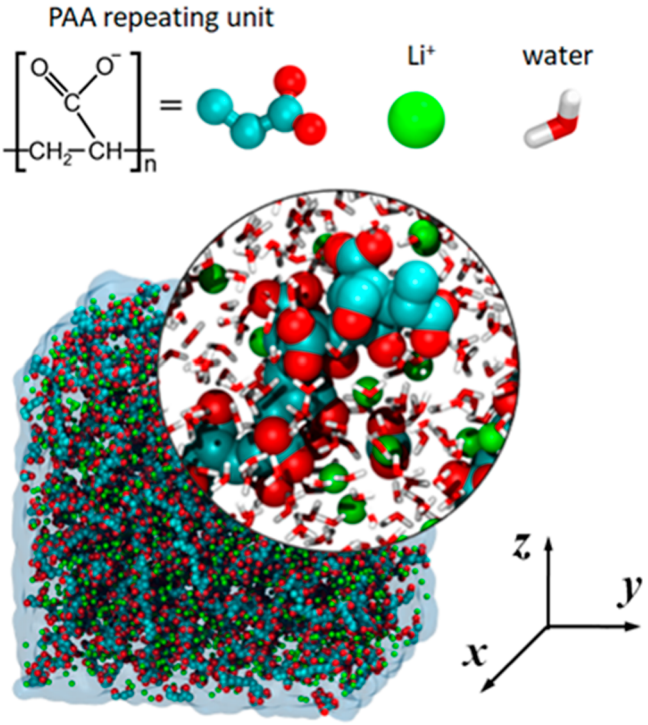

Figure 1. Molecular visualization of a PAA−Li^+−water system. This snapshot was rendered with VMD (Visual Molecular Dynamics[37]). The circle presents an enlarged view of the local atomic configuration of the system. The red ball is the oxygen atom, white is the hydrogen atom, cyan is the carbon atom, and green is Li^+. The chemical formula and its molecular visualization PAA repeating unit present the configuration in which all acid groups are ionized in the electrolyte. The original PAA repeating unit has a carboxylic group (−COOH).

4. RESULTS AND DISCUSSION

4.1. Ionic Conductivity. Figure 2(a) shows a comparison between the conductivities from experiments, σ_{exp}, and those from MD simulations, σ_{MD}, at various ϕ_{Wt}. The ionic conductivity from MD simulations, σ_{MD}, was computed from the Nernst−Einstein relation,[32]

$$\sigma_{MD} = \frac{n_{Li}e^2D_{Li}}{k_BT} \quad (4)$$

where n_{Li} and D_{Li} are the number density and diffusion coefficient of Li ions, respectively, T is the system temperature, e is the elementary charge, and k_B is the Boltzmann constant. This formula indicates that the conductivity of an electrolyte is determined by n_{Li} and D_{Li}. Here, n_{Li} is the system ion concentration, which is associated with the microscopic structure of the electrolyte, while D_{Li} expresses the dynamics of ion mobility. The validity of Nernst−Planck relation in the present system is discussed in Supporting Information, Figure S8.

As observed in Figure 2(a), σ_{MD} agrees very well with σ_{exp}, which confirms the validity of the present MD simulations. Thus, all the discussion in this study is based on the MD simulation results. When the water content is small (ϕ_{Wt} = 0.1), the ionic conductivity is also relatively small (σ_{MD}= 2.84 ± 0.20 × 10^{-4} S/cm). However, the conductivity increases

https://dx.doi.org/10.1021/acsaem.0c01765
ACS Appl. Energy Mater. 2020, 3, 10119−10130

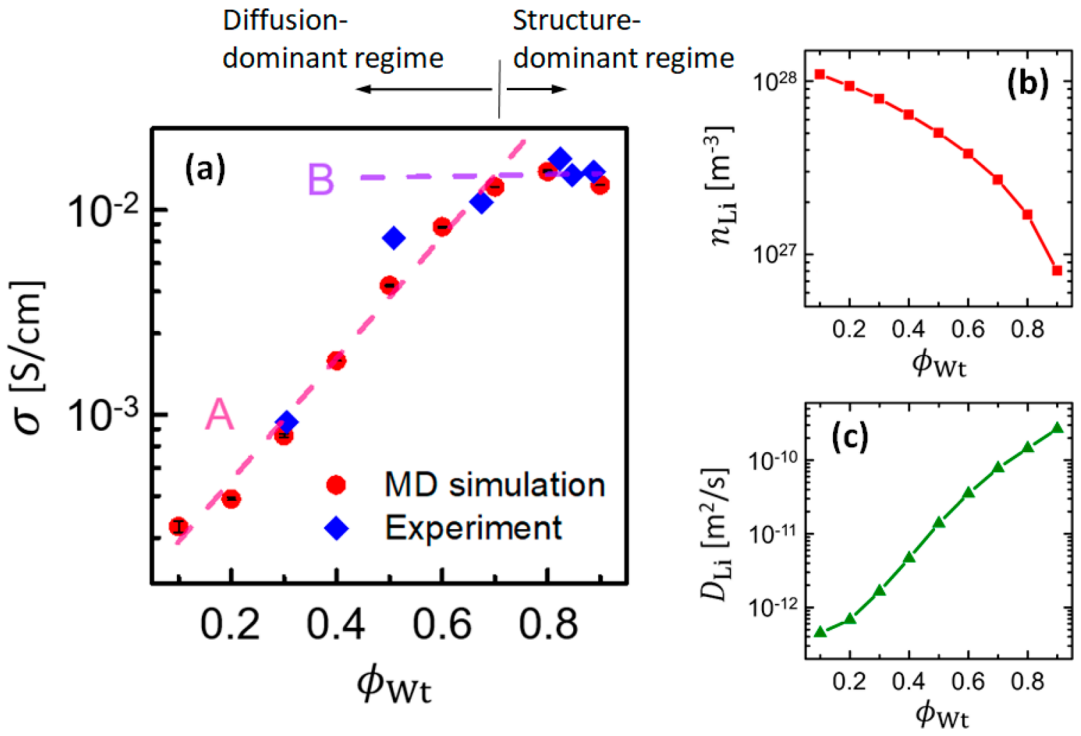

Figure 2. (a) Conductivities of the PAA−Li$^+$−water system from experiments and MD simulations. For both experimental and MD data, the error at each point is less than the symbol size. (b) Change of the number density of Li$^+$ with ϕ_{Wt}. (c) Change of the diffusion coefficient of Li$^+$ with ϕ_{Wt}.

with the addition of water and reaches $\sigma_{MD} = 1.29 \pm 0.014 \times 10^{-2}$ S/cm at $\phi_{Wt} = 0.7$. For $\phi_{Wt} \geq 0.7$ the increment in σ_{MD} becomes insignificant, which is still consistent with σ_{exp}. Hence, the entire MD conductivity profile can be divided into two distinctive regimes, and each section is fitted with a linear line in a log−linear plot (see the dashed lines A and B in Figure 2(a) and eq S1 in the Supporting Information).

Figure 2(b) shows the change of n_{Li} according to ϕ_{Wt}. Here, n_{Li} is a quantity averaged over the whole system. As ϕ_{Wt} increases, n_{Li} decreases. The increase in ϕ_{Wt} brought the expansion of the simulation box, and the box dimensions were determined spontaneously through an equilibrium MD simulation with the NPT ensemble at $p = 1.0$ atm and $T = 300$ K. In other words, the ion and water structures around the polymer were adjusted to minimize the total energy of the system, and a simulation domain with an optimized size was created while achieving equilibrium. When the amount of water in the system varies, the microstructures of ions and water near polymers are modulated in ways that form a new hydration configuration around ions. It leads to a local change in the specific volume of water, and new system dimensions and n_{Li} are settled.

Figure 2(c) reveals the change of D_{Li} depending on ϕ_{Wt}. The diffusion coefficient was determined as the slope of the MSD (mean-square-displacement) plot at long-time limit: $D_{Li} = \lim_{t' \to \infty} \frac{\langle [\mathbf{r}_{Li}(t+t') - \mathbf{r}_{Li}(t)]^2 \rangle}{6t'}$, where $\mathbf{r}_{Li}(t)$ is the instantaneous position of Li$^+$, t' the lag time, and $\langle \cdots \rangle$ denotes an ensemble average—the MSD plots for all ϕ_{Wt}s are shown in Figure S9. Opposite to the behavior of n_{Li}, D_{Li} increases in proportional to ϕ_{Wt} in the log−linear plot.

From the observations of n_{Li} and D_{Li}, we can conclude that the fast increase in conductivity for $\phi_{Wt} < 0.7$ is dominated by the diffusion, while the slow increase in the higher-water-content environment with $\phi_{Wt} \geq 0.7$ is due to a decrease in n_{Li}. Therefore, in the present study, the low-water-content condition with $\phi_{Wt} < 0.7$ is referred to as the *diffusion-dominant regime*, while the water environment with $\phi_{Wt} \geq 0.7$ is denoted as the *structure-dominant regime*. In other words, the diffusion-dominant region and the structure-dominant region are solely distinguished based on the conduction behavior. As shown in Figure 2(a), in the range of $\phi_{Wt} \geq 0.7$, the increase in conductivity shrinks to be negligible, whereas the diffusion coefficient increases still apparently. Therefore, it can be thought that the sudden slow-down of increasing rate originates from the decrease in number density.

4.2. Binding Configurations between Li$^+$ and PAA. A conventional approach to understanding the diffusion behavior of PAA−Li$^+$−water electrolytes is to consider the binding configurations between Li$^+$ and PAA. In order to quantify the configuration, we introduce the binding index, N_O^{bind}, which is defined as the number of PAA oxygen atoms bound to Li$^+$.[33] If the distance between a Li$^+$ and a target oxygen atom in PAA is smaller than a critical value of $d_{eq} = r_{eq} + \sigma_{Li-O}$, the Li$^+$ is regarded as being bound to the oxygen atom. Here, r_{eq} is the equilibrium distance between the Li$^+$ and oxygen atom in the PAA segment (COO^-) in the binding status. The value of r_{eq} is 0.208 nm, which was determined as the first peak position in the RDF for Li$^+$ with respect to the oxygen atoms in PAA. σ_{Li-O} is the σ-value in LJ parameters for the Li$^+$−O pair. Figure 3(a) visualizes the Li$^+$ −O binding configurations with diverse N_O^{bind}s. In the bulk, the Li$^+$ does not have any binding to PAA oxygen atoms, and N_O^{bind} has zero value. Note that four water molecules were displayed in Figure 3(a) with $N_O^{bind} = 0$, since the average hydration number of Li$^+$ in bulk is about 4.[11,12] However, as Li$^+$ approaches to PAA, a binding is formed, and N_O^{bind} becomes nonzero. In the Li$^+$−O binding with $N_O^{bind} = 1$, the ion wanders freely around oxygen atom while keeping a

https://dx.doi.org/10.1021/acsaem.0c01765
ACS Appl. Energy Mater. 2020, 3, 10119−10130

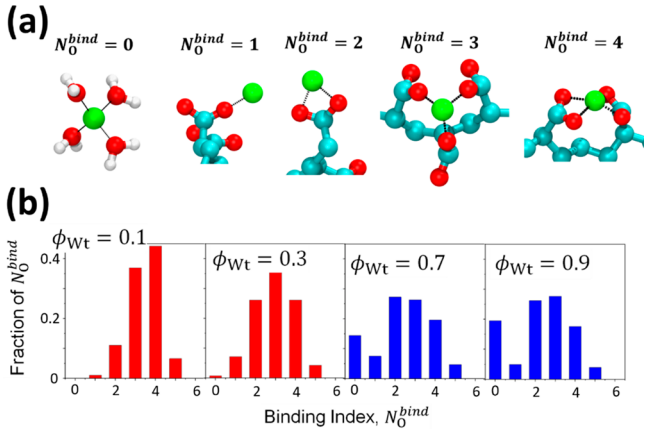

Figure 3. (a) Representative configurations for diverse binding indices of N_O^{bind} = 0, 1, 2, 3, and 4; (b) N_O^{bind} distributions for various water contents of ϕ_{Wt} = 0.1, 0.3, 0.7, and 0.9. The red histograms for ϕ_{Wt} = 0.1 and 0.3 belong to the diffusion-dominant regime. The blue histograms for ϕ_{Wt} = 0.7 and 0.9 belong to the structure-dominant regime, in which the distributions do not change. Complete set of distributions for $0.1 \leq \phi_{Wt} \leq 0.9$ is given in Figure S10 in the Supporting Information.

constant distance. For N_O^{bind} = 2, the Li ion is bound to two oxygen atoms from the same PAA monomer. However, for N_O^{bind} > 2, the ion is surrounded by multiple adjacent PAA segments. If a Li^+ has N_O^{bind} = 3, three adjacent COO^- groups participate in the binding, and each group supplies one oxygen only. If the binding index is large like N_O^{bind} = 4, the oxygen atoms can be from different PAA monomers. For the present system, the bindings in which N_O^{bind} > 6 are hardly found. Since the binding between Li^+ and PAA is formed through Li^+−O bindings, N_O^{bind} also represents the binding strength between Li^+ and PAA polymer. In the present work, the Li ions in the system were regrouped as *free* Li^+ with N_O^{bind} = 0 and *bound* Li^+ with $N_O^{bind} \geq 1$.

The visual information in Figure 3(a) can be quantitatively analyzed by plotting the fractional distributions of N_O^{bind} as shown in Figure 3(b). When the water content is small as ϕ_{Wt} = 0.1, most Li^+ strongly interact with the polymers, and the majority of Li^+ have a binding index of N_O^{bind} = 3 or 4. In such a low water content, the PAA polymer chains are deformed so that the Li^+ can be easily bound to the multiple COO^- segments. When water is added, the polymer chains unfold, and the binding with the oxygen atoms from different PAA chains gets disturbed. For instance, for N_O^{bind} = 3, every oxygen atom comes one by one from adjacent monomers in the same PAA chain (see Figure 3(a)). For the unfolded polymer, the water molecules can easily intervene in the Li^+−O pair, weakening the binding by increasing the Li^+−O distance, and eventually, the N_O^{bind} of that Li^+ is reduced. First, the decrease of the binding with N_O^{bind} = 3, 4 transferred to the bindings with N_O^{bind} = 2 ($0.1 \leq \phi_{Wt} \leq 0.4$). Then, the fraction of N_O^{bind} = 0 grew until saturation ($0.5 \leq \phi_{Wt} \leq 0.7$). The change in the fraction of N_O^{bind} = 1 is not considerable. Because the two oxygen atoms are located close to each other in one monomer unit, the binding with N_O^{bind} = 2 is preferred as opposed to the single-oxygen binding (N_O^{bind} = 1). Overall, it can be said that the release of Li ions happens like the jumps with a step size of 2: When N_O^{bind} is reduced from 4 to 0, its process is 4 → 2 → 0, not 4 → 3 → 2 → 1 → 0. For high water content with $\phi_{Wt} \geq 0.7$, the N_O^{bind} distribution remains unchanged, which corresponds to the sudden slow-down of increment of the conductivity in the structure-dominant regime (see Figure 2(a)).

4.3. Diffusion of Li Ion. Figure 4(a) shows the fractions of bound and free Li^+ as a function of water content. Initially

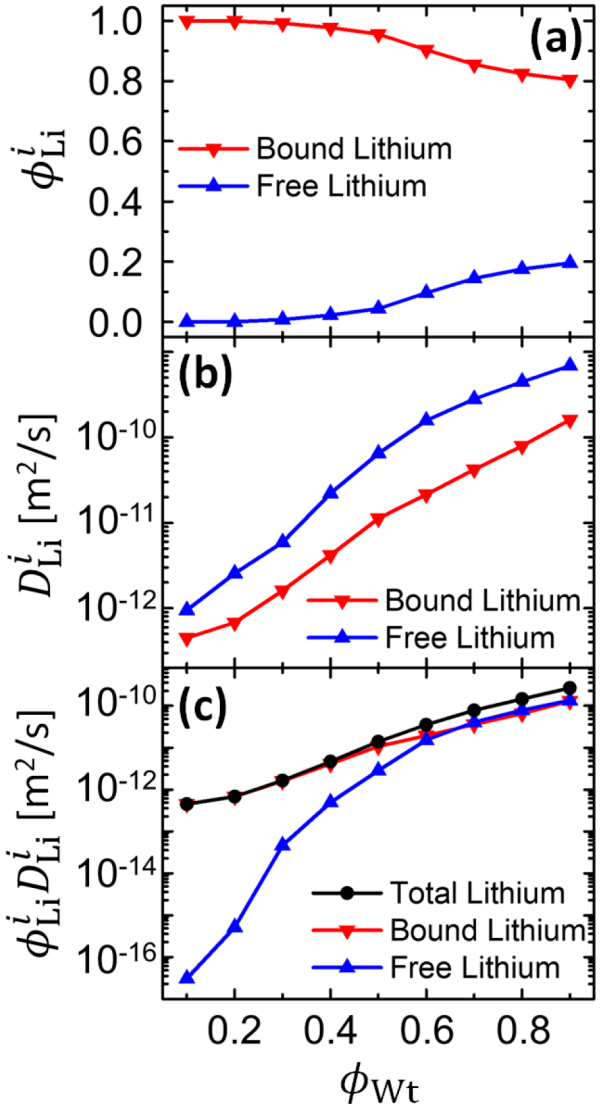

Figure 4. (a) Changes of fractions of free and bound Li^+ with ϕ_{Wt}. (b) Changes of diffusion coefficients of free and bound Li^+ with ϕ_{Wt}. (c) Changes in the contributions of free and bound Li^+ to total Li^+ diffusion with ϕ_{Wt}.

(when ϕ_{Wt} = 0.1), most Li^+ were bound to the PAA polymer. In the diffusion-dominant regime ($\phi_{Wt} < 0.7$), with the addition of water, the fraction of bound Li^+, ϕ_{Li}^{bound}, decreases from 0.99997 at ϕ_{Wt} = 0.1 to 0.8554 at ϕ_{Wt} = 0.7, whereas the fraction of free Li^+, ϕ_{Li}^{free}, is on the rise from 3.23×10^{-5} at ϕ_{Wt} = 0.1 to 0.1446 at ϕ_{Wt} = 0.7. In the structure-dominant regime ($\phi_{Wt} \geq 0.7$), the changes in ϕ_{Li}^{bound} and ϕ_{Li}^{free} become slower. Hence, the maximum ϕ_{Li}^{free}-value achieves only 0.1955, even in a very high-water-content environment (ϕ_{Wt} = 0.9). These observations suggest that the interaction between the polymer and Li^+ is strong enough to overwhelm the solvation-induced attraction toward the outer water-rich zone. The solvation-induced attraction is induced by the tendency of ions to be solvated in bulk water. Thus, even with sufficient water, a large

https://dx.doi.org/10.1021/acsaem.0c01765
ACS Appl. Energy Mater. 2020, 3, 10119−10130

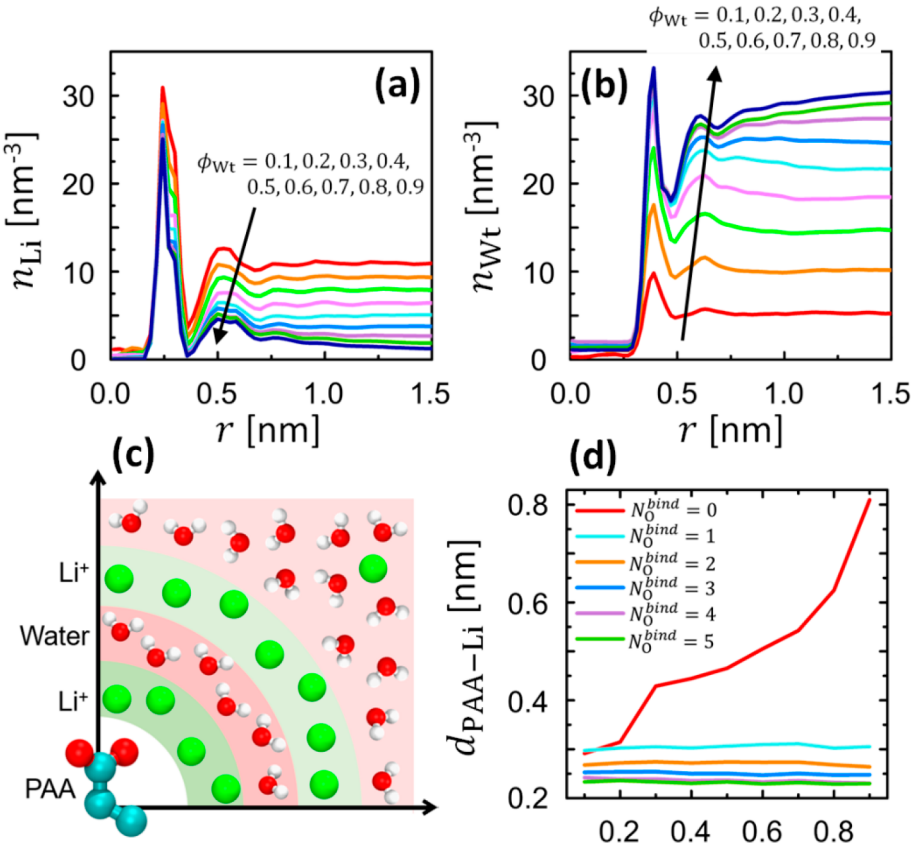

Figure 5. (a) Changes of Li^+ number density distribution with ϕ_{Wt}. (b) Changes of water number density distribution with ϕ_{Wt}. (c) Schematic of Li^+ and water configuration around a PAA monomer. (d) Average equilibrium distance between Li^+ and the mass center of a PAA monomer for diverse binding indices.

number of Li^+ remain near the polymer. Of course, some Li^+ escape the binding area to become free ions, as seen in the change of ϕ_{Li}^{free}.

Figure 4(b) compares the diffusion coefficients of free and bound Li^+. Both diffusion coefficients increase steadily as the amount of water in the system increases. However, the contributions of free and bound Li^+ on the total Li^+ diffusion should be identified with $\phi_{Li}^{bound}D_{Li}^{bound}$ and $\phi_{Li}^{free}D_{Li}^{free}$, because the total Li^+ diffusion coefficient, D_{Li}, is given as $D_{Li} = \phi_{Li}^{bound}D_{Li}^{bound} + \phi_{Li}^{free}D_{Li}^{free}$. As seen in Figure 4(c), although the contribution of free Li^+ is 10^4 times smaller than that of bound Li^+ at ϕ_{Wt} = 0.1, the increment of $\phi_{Li}^{free}D_{Li}^{free}$ according to ϕ_{Wt} is much faster than the rising rate of $\phi_{Li}^{bound}D_{Li}^{bound}$. Then, $\phi_{Li}^{free}D_{Li}^{free}$ becomes identical to $\phi_{Li}^{bound}D_{Li}^{bound}$ at $\phi_{Wt} \approx 0.7$. For the bound Li^+, the contribution steadily increases in proportion to ϕ_{Wt} across the entire range of ϕ_{Wt}, which can be fitted with a single line (see eq S2). However, increasing rate of the contribution of free Li^+ considerably decreases with increasing ϕ_{Wt}, so that the entire $\phi_{Li}^{free}D_{Li}^{free}$ profile can be fitted with three distinctive straight lines (see eq S3). In summary, for $\phi_{Wt} < 0.7$, the bound Li^+ govern the ion conductivity, while for $\phi_{Wt} \geq 0.7$, the conductivity is attributable to both free and bound Li^+.

Although the conventional study based on *free* and *bound* ions unveiled many details in the transport of Li^+ through the PAA−Li−water electrolyte, we still had fundamental questions as follows: (1) Why do the diffusion coefficients increase steadily throughout the entire range of water content, while ϕ_{Li}^{free} and ϕ_{Li}^{bound} are saturated in the structure-dominant regime? (2) What is the physical meaning of ϕ_{Wt} = 0.7, at which the contribution of free Li^+ becomes identical to that of bound Li^+? We felt that these questions could be answered by investigating the ion and water structures around the polymer and their interplay. Next, we focus on the structural properties of the PAA−Li^+−water electrolyte (i.e., microstructures of Li^+ and water around PAA). As mentioned before, the microstructures are closely correlated with n_{Li}.

4.4. Ion and Water Structure around Polymer. Figure 5(a,b) presents the number density distributions of Li^+ and water around a PAA monomer, respectively. Overall, with an increase in ϕ_{Wt}, n_{Li} decreases, whereas the number density of water, n_{Wt}, increases. As mentioned already, the simulation box expanded with the addition of water, which caused an overall decrease in the number density of Li^+ and n_{Li}. However, for n_{Wt}, the increase in the number of water molecules was more influential than the change in volume; thus, n_{Wt} increased. The changes in n_{Li} and n_{Wt} were considerably lessened in the structure-dominant regime ($\phi_{Wt} \geq 0.7$). For Li^+, the density at the second peak ($r \approx 0.5$ nm) dropped from 12.62 nm^{-3} at ϕ_{Wt} = 0.1 to 4.60 nm^{-3} at ϕ_{Wt}= 0.9, while the bulk density ($r > 1.2$ nm) was reduced from 11.00 nm^{-3} at ϕ_{Wt} = 0.1 to 1.00 nm^{-3} at ϕ_{Wt} = 0.9. However, the effects of water addition on the first peak were not very important. In this case, n_{Li} at the first peak ($r \approx 0.24$ nm) appeared as 30.90 nm^{-3} at ϕ_{Wt} = 0.1 and 25.06 nm^{-3} at ϕ_{Wt} = 0.9. These observations confirm that the Li^+ in the first peak were tightly bound to the polymer so that they were not easily released, even though more water molecules were added. Instead, those additional water molecules pushed the Li ions in the first valley ($r \approx 0.36$ nm) to the bulk, causing a 10-fold decrease in the Li-ion density at $r \approx 0.36$ nm (n_{Li} = 3.55 nm^{-3} at ϕ_{Wt} = 0.1 to n_{Li} = 0.41 nm^{-3} at ϕ_{Wt} = 0.9).

https://dx.doi.org/10.1021/acsaem.0c01765
ACS Appl. Energy Mater. 2020, 3, 10119−10130

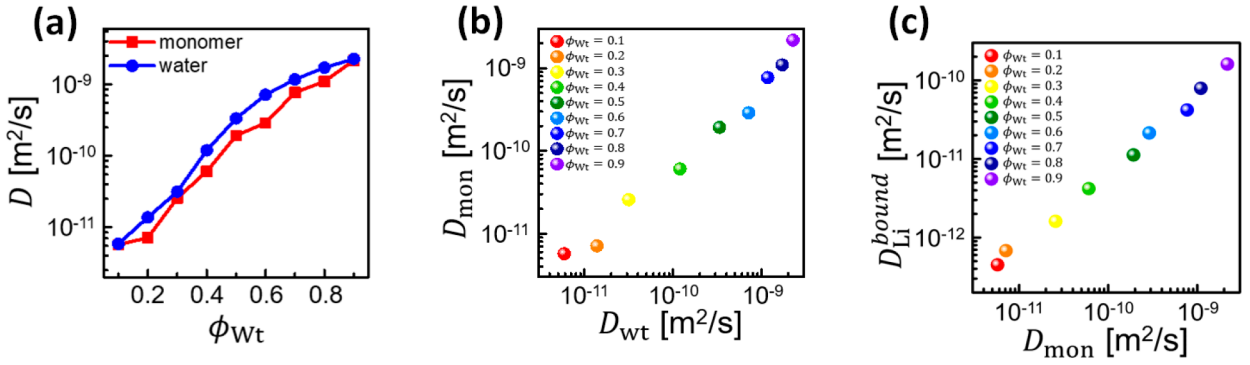

Figure 6. (a) Change of diffusion coefficients of PAA monomer and water depending on water content, ϕ_{Wt}. (b) Correlation between the dynamics of water and the diffusional motion of the PAA monomer. D_{mon} is the diffusion coefficient of the PAA monomer. (c) Correlation between the dynamics of the bound lithium ion, D_{Li}^{bound}, and the diffusional motion of the PAA monomer, D_{mon}.

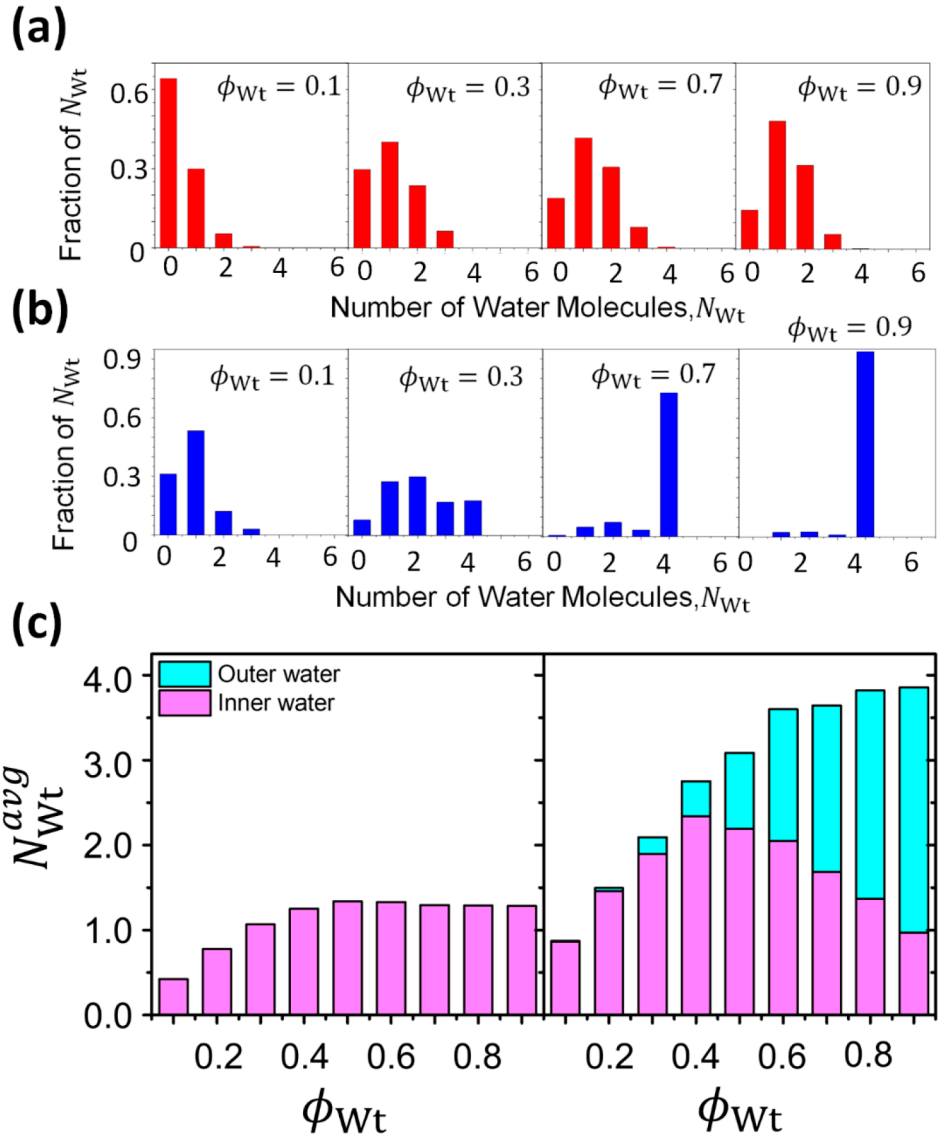

Figure 7. (a) N_{Wt} distributions for inner Li^+ depending on water contents of ϕ_{Wt} = 0.1, 0.3, 0.7, and 0.9. Complete set of distributions for 0.1 ≤ ϕ_{Wt} ≤ 0.9 is given in Figure S13. (b) N_{Wt} distributions for outer Li^+ depending on water content with ϕ_{Wt} = 0.1, 0.3, 0.7, and 0.9. A complete set of distributions for 0.1 ≤ ϕ_{Wt} ≤ 0.9 is given in Figure S14. (c) Variation of average hydration number for inner Li^+ (left) and outer Li^+ (right) according to ϕ_{Wt}. Different colors express the contributions from inner and outer water.

https://dx.doi.org/10.1021/acsaem.0c01765
ACS Appl. Energy Mater. 2020, 3, 10119−10130

Different from n_{Li} in the first peak, n_{Li} in the second peak was readily influenced by the water addition, because the binding by PAA chains is weak.

The responses of n_{Wt} to water addition are opposite to those of n_{Li} (i.e., n_{Wt} increased uniformly across the entire domain as ϕ_{Wt} increases). At the second peak ($r \approx 0.62$ nm), n_{Wt} increased from 5.74 nm^{-3} at $\phi_{Wt} = 0.1$ to 27.68 nm^{-3} at $\phi_{Wt} = 0.9$, while n_{Wt} in the bulk region ($r > 1.2$ nm) rose from 5.28 nm^{-3} at $\phi_{Wt} = 0.1$ to 30.93 nm^{-3} at $\phi_{Wt} = 0.9$. The second peak was imperceptible initially in the low-water-content condition but grew rapidly with the addition of water. Moreover, the first peak ($r \approx 0.39$ nm), which was initially a small bump in the profile, grew from 9.83 nm^{-3} at $\phi_{Wt} = 0.1$ to 33.13 nm^{-3} at $\phi_{Wt} = 0.9$. Despite those considerable changes in magnitude, the peak and valley positions in n_{Li} and n_{Wt} varied little with ϕ_{Wt}. This can be clearly recognized by looking at the radial distribution functions (RDFs) for Li^+ and water together (see Figure S11). From Figure S11, we find that the peak and valley positions are preserved regardless of the addition of water. The Li^+-rich region and water-rich zone alternate around PAA, as schematically displayed in Figure 5(c). First, the positive Li^+ attach to the negative COO^- in the PAA monomer due to strong electrostatic attraction. Then, the water molecules become arranged outside the Li^+-rich zone with the oxygen atoms oriented toward the Li^+. In the immediate vicinity of the polymer, the Li^+ and water molecules cannot be located very close to each other due to geometric hindrance by finite ion size.

Figure 5(d) shows an average equilibrium distance of Li^+ from the center of a PAA monomer according to N_O^{bind}. All the distances varied little except the case with $N_O^{bind} = 0$. In other words, the initial positions of bound Li^+ determined in a low-water-content environment are affected little by water addition. This yields the location-fixed first peaks in Figure 5(a). However, the equilibrium distance of the Li^+ located away from the polymer ($N_O^{bind} = 0$) rapidly increases with the addition of water, because the strong solvation tendency pushes the ions toward the bulk. This observation implies that once the Li^+ are properly coordinated with PAA polymer, they are not easily released from their binding sites (i.e., the PAA−Li^+ interaction is stronger than the solvation tendency of Li^+).

Here, we need to introduce the concepts of inner water and outer water. In the present study, the water inside the first hydration shell of polymer is called *inner* water, while the water outside the first shell is referred to as *outer* water. The inner and outer water each have a number of features (see Figure S12): (1) Only after the PAA−Li^+ complex is fully solvated, a significant portion of the added water begins to fill the region outside the first hydration shell. (2) The fractions of inner and outer waters cross at $\phi_{Wt} \approx 0.7$, at which the conductivity is saturated, and $\phi_{Li}^{bound} D_{Li}^{bound}$ becomes identical to $\phi_{Li}^{free} D_{Li}^{free}$. (3) The diffusion coefficient of the inner water, D_{Wt}^{in}, is always lower than that of the outer water, D_{Wt}^{out}, because the strong solvation characteristics of the PAA−Li^+ complex immobilize the surrounding water molecules.

As with the water classification, the Li^+ in the system also can be distinguished as *inner* and *outer* Li^+. A Li ion is considered inner Li^+ when it stays in the inner water, while outer Li^+ consists of Li ions reside in the outer water. Interestingly, *the inner Li^+mostly correspond to the bound ones, while the outer $Li^+$are largely equivalent to free ones*. As seen in Figure 5(d), all the distances between bound Li^+ and a PAA monomer are smaller than 0.3 nm regardless of the water content, and this value is almost the same as the radius of the first hydration shell (see Figure 5(b)). However, the distance between free Li^+ and a PAA monomer increases with an increase in ϕ_{Wt}, which implies that the free Li^+ stays outside the hydration shell except in the lowest-water-content environment ($\phi_{Wt} \leq 0.2$).

Figure 6 presents the influence of water content on the diffusion of the PAA monomer and water (Figure 6(a)), the correlation between D_{Wt} and D_{mon} (Figure 6(b)), and the correlation between D_{Li}^{bound} and D_{mon} (Figure 6(c)). The diffusion of the PAA monomer and water increases in proportion to water content and the diffusion coefficient of water, and the diffusion of bound lithium ion increases with the increases in the diffusion of monomer. In other words, as the water is added, the diffusion coefficient of water increases, which incurs the increase of the diffusion of PAA monomer; subsequently, the stronger diffusion of PAA monomer enhances the dynamics of PAA monomers.

4.5. Ion Hydration Structures. Figure 7(a,b) depicts the distributions of hydration numbers for inner and outer Li^+, respectively. The hydration number, N_{Wt}, is defined as the number of water molecules within the radius of the first hydration shell of the Li ion (~0.25 nm). For the inner Li^+, at $\phi_{Wt} = 0.1$, the fractions are given as $\phi_{Li}^0/\phi_{Li}^1/\phi_{Li}^2 = 0.641{:}0.300{:}0.053$, where ϕ_{Li}^i is the fraction of Li^+ with $N_{Wt} = i$ (see Figure 7(a)). In such a low-water-content environment, the majority of Li^+ was completely absorbed without any intervention of water molecules ($N_{Wt} = 0$). With the addition of water, ϕ_{Li}^2 significantly increases as ϕ_{Li}^0 decreases: at $\phi_{Wt} = 0.7$, the distribution appears to be $\phi_{Li}^0/\phi_{Li}^1/\phi_{Li}^2 = 0.190{:}0.417{:}0.308$. Namely, the inner Li ions without surrounding water acquire two water molecules at once upon the addition of water. This implies that for the Li^+ with $N_{Wt} = 0$, it is more energetically favorable to coordinate two water molecules than one. The coordination with $N_{Wt} > 2$ is hardly permitted because of the geometric hindrance. Noticeably, the Li^+ with $N_{Wt} = 1$ always remain in the majority over the other types of ions except in the case of $\phi_{Wt} = 0.1$. Figure 7(b) presents the N_{Wt} distribution for outer Li^+. At $\phi_{Wt} = 0.1$, $\phi_{Li}^0/\phi_{Li}^1/\phi_{Li}^2/\phi_{Li}^3 = 0.313{:}0.533{:}0.122{:}0.032$. With the addition of water to $\phi_{Wt} = 0.3$, ϕ_{Li}^2 increased as ϕ_{Li}^0 and ϕ_{Li}^1 decreased. The fraction with $N_{Wt} = 4$ started to increase rapidly at $\phi_{Wt} = 0.3$, where the sudden changes in ϕ_{Li}^{free} and ϕ_{Li}^{bound} start (see Figure 4(a)). Because fully hydrated Li^+ has $N_{Wt} = 4$,[11,12] the increment in ϕ_{Li}^4 can be interpreted as that more and more ions have a bulk-like environment (see Figure 3(a)). The increment became remarkably slower in the structure-dominant regime.

Figure 7(c) compares the average hydration numbers, N_{Wt}^{avg}, for inner and outer Li ions. The portions of pink and cyan colors express the contributions of inner and outer waters, respectively, to N_{Wt}^{avg}. In the figure, N_{Wt}^{avg} becomes saturated as 1.30 at $\phi_{Wt} = 0.5$ for inner Li^+, while N_{Wt}^{avg} achieves 3.73 at $\phi_{Wt} = 0.6$ for outer Li^+. The small N_{Wt}^{avg} explains the slow diffusion of inner Li^+, because N_{Wt}^{avg} represents the mean number of water molecules colliding with ions to induce random motion of ions. Moreover, the inner Li^+ are mostly surrounded by the slower-moving inner waters.

Different from the inner Li^+, the outer Li^+ are affected by both inner and outer water. Initially, at $\phi_{Wt} = 0.1$ and 0.2, N_{Wt}^{avg} is mostly determined by the inner water, because the Li^+ are so closely packed in the near vicinity of the polymer that their interaction with the outer water is weak. The average hydration number by inner water $N_{Wt}^{in,avg}$ ($r < 0.35$ nm), increases until

https://dx.doi.org/10.1021/acsaem.0c01765
ACS Appl. Energy Mater. 2020, 3, 10119−10130

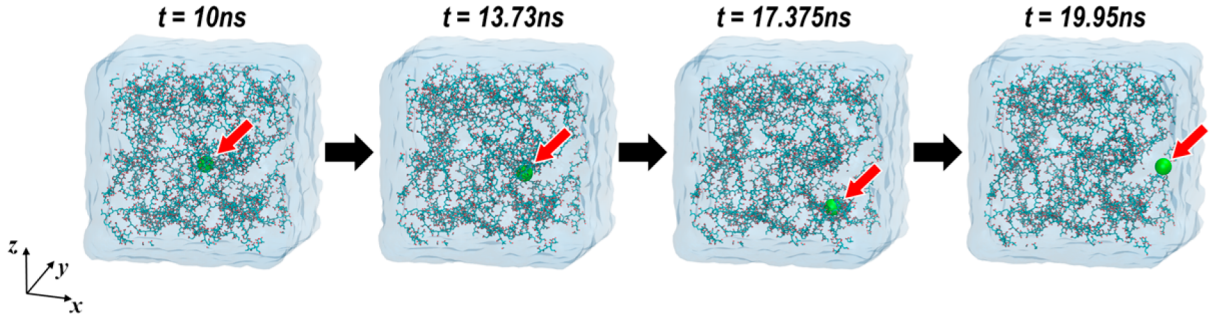

Figure 8. Visualization of Li^+ transport through the water channel in the PAA−Li^+−water system with $\phi_{Wt} = 0.7$ under an E field of $E = 0.01$ V/nm. Only the PAA polymers and a typical single Li^+ are presented, while the other Li^+ and water molecules are not shown.

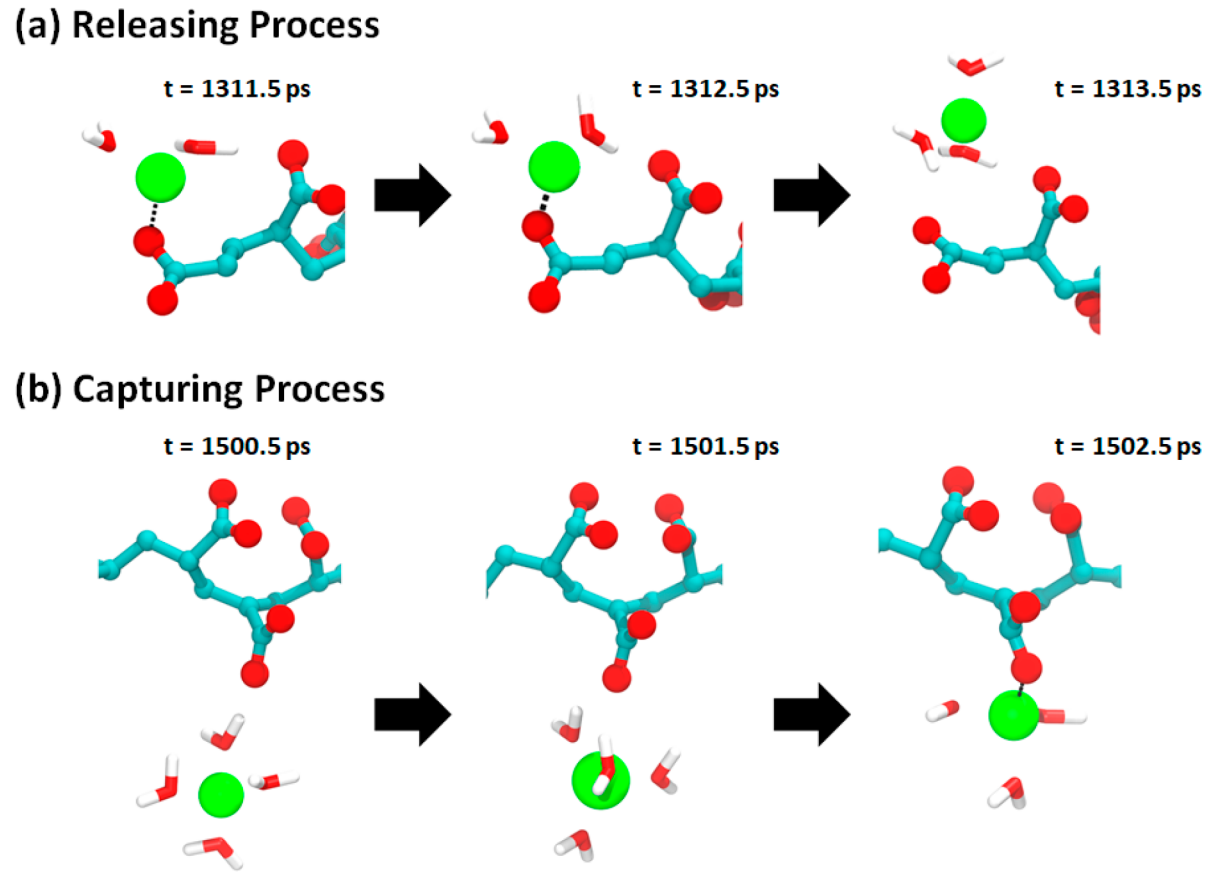

Figure 9. (a) Releasing and (b) capturing of Li^+ by PAA polymer at a high-water-content condition.

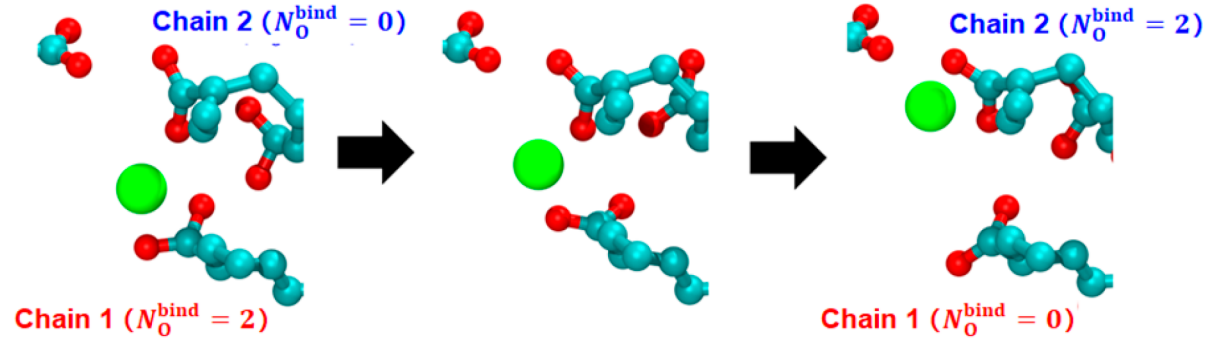

Figure 10. Schematic of ion transport through present APE at low water content ($\phi_{Wt} = 0.3$).

reaching the maximum at $\phi_{Wt} = 0.4$; it then decreases with a further increase in ϕ_{Wt}. The hydration number of the faster-moving outer water, $N_{Wt}^{out,avg}$, which is negligible at $\phi_{Wt} = 0.1$ and 0.2, steadily increases with an increase in ϕ_{Wt} (starting

https://dx.doi.org/10.1021/acsaem.0c01765
ACS Appl. Energy Mater. 2020, 3, 10119−10130

from ϕ_{Wt} = 0.3). This produced a steady increase in D_{Li}^{free} outside the first hydration shell regardless of the saturation of the fraction of free Li^+ (see Figure 4(a)). Here, it should be noted again that the free Li^+ are mostly placed outside the first hydration shell. However, even at a very high water content (ϕ_{Wt} = 0.9), D_{Li}^{free} did not reach the value at infinite dilution in water,[11,12] because the contribution of the slower inner water did not vanish completely.

4.6. Ion Migration Mechanism. In order to further understand the transport mechanism of Li^+ in the present electrolyte, we visualized the migration of a typical Li^+ through medium under an electric field of E = 0.01 V/nm for ϕ_{Wt} = 0.7. The movie file is presented in the Supporting Information. The snapshots of the movie are also shown in Figure 8. In the figure, we can clearly observe that a water channel is formed,[34] which acts as a passage for ion transport. As seen in the movie and the snapshots, at the high-water-content condition, a Li^+ ion bound to the oxygen atoms in the PAA polymer is released from the polymer by hydration to form a free ion (releasing process), travels the water channel freely, and is then trapped again by another PAA polymer (trapping process). Those releasing and trapping processes at high water content are shown in Figure 9. Different from the process at high water content, when the water content is low as ϕ_{Wt} = 0.3, the lithium ions travel by jumping from one to another PAA polymer chains without solvation in water (see Figure 10).[35] However, as the water is added and ϕ_{Wt} increases, the role of water becomes significant: The bound ion is released by hydration, and the free ion travels the water tube with large mobility.

The proposed electrolyte may have a low electrochemical window due to the larger water content. However, in the present study, we focused on a molecular-level understanding of the structural (ion/water distribution around the polymer) and dynamic (diffusion coefficient) properties of the PAA-based APE to develop highly conducting, flexible, and stable electrolytes. With the knowledge of how to design the high-conductivity APE, the addition of lithium salt to the electrolyte (such as a water-in-salt APE) can be one of the ways to increase an electrochemical window of the APE-based energy storage device. We have found that the lithium-salt incorporation leads to a further increase in ionic conductivity, as indicated by Suo et al.[7] A full experimental and computational report on the electrochemical properties of the lithium-salt-containing APE-based energy storage device will be detailed in a forthcoming publication.

5. CONCLUSIONS

In conclusion, based on experiments and extensive MD simulations, we found that the conductivity of the polymer–Li^+–water electrolyte was able to increase to about 10^{-2} S/cm by employing strongly hydrophilic PAA as its polymer matrix, functionalizing lithium cations as mobile ions, and making the water content optimal. The change in conductivity according to ϕ_{Wt} was divided into the diffusion-dominant regime at the low-water-content condition (ϕ_{Wt} < 0.7) and the structure-dominant regime at the high-water-content condition ($\phi_{Wt} \geq$ 0.7). In the diffusion-dominant regime, the conductivity was increased by diffusion enhancement proportional to the water content, while in the structure-dominant regime, the conductivity varied little due to the considerable reduction of the number density of Li^+. The rigorous understanding of the steady increase in free and bound ion diffusions and the constant decrease in the number density of Li^+ across the entire ϕ_{Wt} range was possible only when the microscopic interaction between ions, water, and polymers was considered instead of the classical approach based on free ions.[24] When water was introduced, the added water went to both the outside and the inside of the first hydration shell of PAA. The inner Li^+ were always dissolved in the slower inner water (inside the first hydration shell of polymer), and $N_{Wt}^{in,avg}$ was increased to 1.3. However, for the outer Li^+, the fraction of the fast-moving outer water in their surroundings rapidly increased as ϕ_{Wt} increased, and $N_{Wt}^{out,\ avg}$ became close to 4. Such strong hydration with faster-moving water brought about the gigantic increase in the outer, and subsequently total, ion diffusion. At ϕ_{Wt} = 0.7, the fraction of inner water became identical with that of outer water. For ϕ_{Wt} < 0.7, PAA polymer was able to absorb water, and as a result, the electrolyte's structural characteristics including N_O^{bind}, $\phi_{Li}^{bound(free)}$, and $N_{Wt}^{in(out)}$ were altered according to ϕ_{Wt}. For $\phi_{Wt} \geq$ 0.7, the amount of water exceeded the polymer's water absorption capacity and the excess waters in the outer region did not interact with the ion–water structure near the polymer. This caused the system volume to expand and the ion number density to shrink considerably.

Considering that the structural stiffness of APE could be weakened by the addition of water, the observations in the present study will be greatly helpful in optimizing water content to achieve a rigid electrolyte while maximizing its conductivity. Also, the proposed PAA-based APE may not be used for Li metal batteries due to the electrolyte containing water. However, the APE can be used as an electrolyte for an aqueous rechargeable lithium-ion battery (ARLB), which was invented in 1994 using an aqueous electrolyte, a $LiMn_2O_4$ cathode, and a VO_2(B) anode.[36] Therefore, the proposed nontoxic and flexible APE could offer a promising solution for the development of flexible and wearable aqueous rechargeable lithium-ion batteries that would have wide applications in displays, wireless sensors, and implantable medical devices.[21]

■ ASSOCIATED CONTENT

Supporting Information

The Supporting Information is available free of charge at https://pubs.acs.org/doi/10.1021/acsaem.0c01765.

Ionic conductivity measurement, size of vinyl silica nanoparticles (VSNs), extent of neutralization with lithium cations in the electrolyte, compositions of polymer, nanoparticle, and water, molecular weight and lengths of PAA strands between nanoparticles, glass transition temperature, silica nanoparticle distribution within PAA matrix, pH measurement, validity of Nernst–Einstein equation, line fits, MSD plots, distribution of N_O^{bind}, RDFs of Li^+ and water around a PAA monomer, inner vs. outer water, distribution of N_{Wt}^{in}, distribution of N_{Wt}^{out} (PDF)

Migration of a typical Li^+ through medium under an electric field of E = 0.01 V/nm for ϕ_{Wt} = 0.7 (MP4)

■ AUTHOR INFORMATION

Corresponding Authors

Jaekwang Lee – *Department of Physics, Pusan National University, Busan 46241, South Korea*; Email: jaekwangl@pusan.ac.kr

https://dx.doi.org/10.1021/acsaem.0c01765
ACS Appl. Energy Mater. 2020, 3, 10119–10130

U Hyeok Choi − *Department of Polymer Science and Engineering, Inha University, Incheon 22212, South Korea;* orcid.org/0000-0002-0048-9550; Email: uhyeok@inha.ac.kr

Authors

Jae Hyun Park − *Department of Aerospace and Software Engineering, Gyeongsang National University, Jinju, Gyeongnam 52828, South Korea;* orcid.org/0000-0003-1418-5897

Sungyeb Jung − *Department of Physics, Pusan National University, Busan 46241, South Korea*

Yeon Hwa Song − *Department of Polymer Engineering, Pukyong National University, Busan 48513, South Korea*

Narayana R. Aluru − *Beckman Institute for Advanced Science and Technology, Department of Mechanical Science and Engineering, University of Illinois at Urbana−Champaign, Urbana, Illinois 61801, United States;* orcid.org/0000-0002-9622-7837

Taehoon Kim − *Composites Research Division, Korea Institute of Materials Science, Changwon, Gyeongnam 51508, South Korea;* orcid.org/0000-0003-1045-616X

Sang Bok Lee − *Composites Research Division, Korea Institute of Materials Science, Changwon, Gyeongnam 51508, South Korea*

Complete contact information is available at: https://pubs.acs.org/10.1021/acsaem.0c01765

Author Contributions

U.H.C. designed the experiments in consultation with J.H.P. and J.L. T.K., S.B.L., and Y.H.S. performed the experiments. J.H.P., J.L., and N.R.A. designed the MD simulations in consultation with T.K. and S.B.L. J.H.P. and S.J. performed the simulations. J.H.P., S.J., J.L., U.H.C., and N.R.A. analyzed the data. J.H.P., S.J., J.L., and U.H.C. cowrote the manuscript, and all of the authors discussed the results and commented on them.

Author Contributions

$^{\nabla}$J.H.P. and S.J. contributed equally.

Notes

The authors declare no competing financial interest.

■ ACKNOWLEDGMENTS

This work was supported by the Fundamental Research Program (PNK6660) of the Korea Institute of Materials Science (KIMS) and partially supported by a National Research Foundation of Korea (NRF) grant funded by the Korea government (MSIT) (No. 2019R1C1C1002161). J.H.P. was supported by the Basic Science Research Program through the National Research Foundation of Korea (NRF) and funded by the Ministry of Education (No. 2014R1A1A2059123).

■ REFERENCES

(1) Armand, M.; Tarascon, J. M. Building Better Batteries. *Nature* **2008**, *451*, 652−657.
(2) Blomgren, G. E. The Development and Future of Lithium Ion Batteries. *J. Electrochem. Soc.* **2017**, *164*, A5019−A5025.
(3) Xu, K. Electrolytes and Interphases in Li-ion Batteries and Beyond. *Chem. Rev.* **2014**, *114*, 11503−11618.
(4) Chen, R.; Qu, W.; Guo, X.; Li, L.; Wu, F. The Pursuit of Solid-State Electrolytes for Lithium Batteries: From Comprehensive Insight to Emerging Horizons. *Mater. Horiz.* **2016**, *3*, 487−516.
(5) Liu, K.; Liu, Y.; Lin, D.; Pei, A.; Cui, Y. Materials for Lithium-ion Battery Safety. *Sci. Adv.* **2018**, *4*, eaas9820.
(6) Eftekhari, A. High-Energy Aqueous Lithium Batteries. *Adv. Energy Mater.* **2018**, *8*, 1801156.
(7) Suo, L.; Borodin, O.; Gao, T.; Olguin, M.; Ho, J.; Fan, X.; Luo, C.; Wang, C.; Xu, K. 'Water-in-Salt' Electrolyte Enables High-Voltage Aqueous Lithium-ion Chemistries. *Science* **2015**, *350*, 938−943.
(8) Song, W.-J.; Lee, S.; Song, G.; Park, S. Stretchable Aqueous Batteries: Progress and Prospects. *ACS Energy Lett.* **2019**, *4*, 177−186.
(9) Hashmi, S. A. Influence of Water Absorption on Poly−Ethylene Oxide-Based Polymer Electrolytes Complexed with Ammonium, Sodium and Magnesium Perchlorates. *J. Mater. Sci.* **1998**, *33*, 989−993.
(10) Tanzella, F.L.; Bailey, W.; Frydrych, D.; Farrington, G. C.; Story, H.S. Ion Transport in Peo-Alkali Salt Complex Polymeric Electrolytes. *Solid State Ionics* **1981**, *5*, 681−684.
(11) Koneshan, S.; Rasaiah, J. C.; Lynden-Bell, R. M.; Lee, S. H. Solvent Structure, Dynamics, and Ion Mobility in Aqueous Solutions at 25 °C. *J. Phys. Chem. B* **1998**, *102*, 4193−4204.
(12) Lee, S. H.; Rasaiah, J. C. Molecular Dynamics Simulation of Ion Mobility. 2. Alkali Metal and Halide Ions Using the SPC/E Model for Water at 25 °C. *J. Phys. Chem.* **1996**, *100*, 1420−1425.
(13) Do, C.; Lunkenheimer, P.; Diddens, D.; Götz, M.; Weiß, M.; Loidl, A.; Sun, X.-G.; Allgaier, J.; Ohl, M. Li^+ Transport in Poly(Ethylene Oxide) Based Electrolytes: Neutron Scattering, Dielectric Spectroscopy, and Molecular Dynamics Simulations. *Phys. Rev. Lett.* **2013**, *111*, 018301.
(14) Zhang, Z.; Ohl, M.; Diallo, S. O.; Jalarvo, N. H.; Hong, K.; Han, Y.; Smith, G. S.; Do, C. Dynamics of Water Associated with Lithium Ions Distributed in Polyethylene Oxide. *Phys. Rev. Lett.* **2015**, *115*, 198301.
(15) Langer, R. Drug Delivery and Targeting. *Nature* **1998**, *392*, 5−10.
(16) Langer, R. Drugs on Target. *Science* **2001**, *293*, 58−59.
(17) Langer, R.; Tirrell, D. A. Designing Materials for Biology and Medicine. *Nature* **2004**, *428*, 487−492.
(18) Krause, T. L.; Bittner, G. D. Rapid Morphological Fusion of Severed Myelinated Axons by Polyethylene Glycol. *Proc. Natl. Acad. Sci. U. S. A.* **1990**, *87*, 1471−1475.
(19) Kim, H.; Hong, J.; Park, K.-Y.; Kim, H.; Kim, S.-W.; Kang, K. Aqueous Rechargeable Li and Na Ion Batteries. *Chem. Rev.* **2014**, *114*, 11788.
(20) Fan, L.; Wei, S.; Li, S.; Li, Q.; Lu, Y. Recent Progress of the Solid-State Electrolytes for High-Energy Metal-Based Batteries. *Adv. Energy Mater.* **2018**, *8*, 1702657.
(21) Yang, C.; Ji, X.; Fan, X.; Gao, T.; Suo, L.; Wnag, F.; Sun, W.; Chen, J.; Chen, L.; Han, F.; Miao, L.; Xu, K.; Gerasopoulos, K.; Wang, C. Flexible Aqueous Li-ion Battery with High Energy and Power Densities. *Adv. Mater.* **2017**, *29*, 1701972.
(22) Baskoro, F.; Wong, H. Q.; Yen, H. J. Strategic Structural Design of a Gel Polymer Electrolyte toward a High Efficiency Lithium-ion Battery. *ACS Appl. Energy Mater.* **2019**, *2*, 3937−3971.
(23) Huang, Y.; Zhong, M.; Huang, Y.; Zhu, M.; Pei, Z.; Wang, Z.; Xue, Q.; Xie, X.; Zhi, C. A Self-Healable and Highly Stretchable Supercapacitor Based on a Dual Crosslinked Polyelectrolyte. *Nat. Commun.* **2015**, *6*, 10310.
(24) Sulatha, M. S.; Natarajan, U. Origin of the Difference in Structural Behavior of Poly(acrylic acid) and Poly(methacrylic acid) in Aqueous Solution Discerned by Explicit-Solvent Explicit-ion MD Simulations. *Ind. Eng. Chem. Res.* **2011**, *50*, 11785−11796.
(25) Berendsen, H. J. C.; Grigera, J. R.; Straatsma, T. P. The Missing Term in Effective Pair Potentials. *J. Phys. Chem.* **1987**, *91*, 6269−6271.
(26) Dang, L. X. Development of Nonadditive Intermolecular Potentials Using Molecular Dynamics: Solvation of Li^+ and F^- ions in Polarizable Water. *J. Chem. Phys.* **1992**, *96*, 6970−6977.
(27) Hess, B.; Kutzner, C.; van der Spoel, D.; Lindahl, E. GROMACS 4: Algorithms for Highly Efficient, Load-Balanced, and

Scalable Molecular Simulation. *J. Chem. Theory Comput.* **2008**, *4*, 435−447.
(28) Hoover, W. G. Canonical Dynamics: Equilibrium Phase-Space Distributions. *Phys. Rev. A: At., Mol., Opt. Phys.* **1985**, *31*, 1695−1697.
(29) Nosé, S. A. Molecular Dynamics Method for Simulations in the Canonical Ensemble. *Mol. Phys.* **1984**, *52*, 255−268.
(30) Parrinello, M.; Rahman, A. Crystal Structure and Pair Potentials: A Molecular-Dynamics Study. *Phys. Rev. Lett.* **1980**, *45*, 1196−1199.
(31) Rahman, A.; Parrinello, M. Polymorphic Transitions in Single Crystals: A New Molecular Dynamics Method. *J. Appl. Phys.* **1981**, *52*, 7182−7190.
(32) Hansen, J.-P.; McDonald, I. *Theory of Simple Liquids: with Applications to Soft Matter*, 4th ed.; Academic Press: Oxford, UK, 2013.
(33) Burlatsky, S.; Darling, R. M.; Novikov, D.; Atrazhev, V. V.; Sultanov, V. I.; Astakhova, T. Y.; Su, L.; Brushett, F. Molecular Dynamics Modeling of the Conductivity of Lithiated Nafion Containing Nonaqueous Solvents. *J. Electrochem. Soc.* **2016**, *163*, A2232−A2239.
(34) Lim, J.; Park, K.; Lee, H.; Kim, J.; Kwak, K.; Cho, M. Nanometric Water Channels in Water-in-Salt Lithium Ion Battery Electrolyte. *J. Am. Chem. Soc.* **2018**, *140*, 15661−15667.
(35) Bresser, D.; Lyonnard, S.; Iojoiu, C.; Picard, L.; Passerini, S. Decoupling Segmental Relaxation and Ionic Conductivity for Lithium-Ion Polymer Electrolytes. *Mol. Syst. Des. Eng.* **2019**, *4*, 779−792.
(36) Li, W.; Dahn, J. R.; Wainwright, D. S. Rechargeable Lithium Batteries with Aqueous Electrolytes. *Science* **1994**, *264*, 1115−1118.
(37) Humphrey, W.; Dalke, A.; Schulten, K. VMD: Visual Molecular Dynamics. *J. Mol. Graphics* **1996**, *14*, 33−38.

https://dx.doi.org/10.1021/acsaem.0c01765
ACS Appl. Energy Mater. 2020, 3, 10119−10130